JOURNAL OF SYNCHROTRON RADIATION
ISSN 1600-5775

Augmentation of the step-by-step Energy-Scanning EXAFS beamline BL-09 to continuous-scan EXAFS mode at INDUS-2 SRS

Ashwini Kumar Poswal,[a]* Ankur Agrawal,[a] Himanshu Kumar Poswal,[b] Dibyendu Bhattacharyya,[a] Shambhu Nath Jha[a] and Naba Kishore Sahoo[a]

[a]Atomic and Molecular Physics Division, Bhabha Atomic Research Centre, Mumbai 400 085, India, and [b]High Pressure and Synchrotron Radiation Physics Division, Bhabha Atomic Research Centre, Mumbai 400 085, India. *Correspondence e-mail: anshu@barc.gov.in

Received 27 April 2016
Accepted 24 August 2016

Edited by J. F. van der Veen

Keywords: time-resolved EXAFS; chemical processes.; quick-XAS; time-resolved EXAFS.

An innovative scheme to carry out continuous-scan X-ray absorption spectroscopy (XAS) measurements similar to quick-EXAFS mode at the Energy-Scanning EXAFS beamline BL-09 at INDUS-2 synchrotron source (Indore, India), which is generally operated in step-by-step scanning mode, is presented. The continuous XAS mode has been implemented by adopting a continuous-scan scheme of the double-crystal monochromator and on-the-fly measurement of incident and transmitted intensities. This enabled a high signal-to-noise ratio to be maintained and the acquisition time was reduced to a few seconds from tens of minutes or hours. The quality of the spectra (signal-to-noise level, resolution and energy calibration) was checked by measuring and analysing XAS spectra of standard metal foils. To demonstrate the energy range covered in a single scan, a continuous-mode XAS spectrum of copper nickel alloy covering both Cu and Ni *K*-edges was recorded. The implementation of continuous-scan XAS mode at BL-09 would expand the use of this beamline in *in situ* time-resolved XAS studies of various important systems of current technological importance. The feasibility of employing this mode of measurement for time-resolved probing of reaction kinetics has been demonstrated by *in situ* XAS measurement on the growth of Ag nanoparticles from a solution phase.

1. Introduction

X-ray absorption spectroscopy (XAS), which deals with the measurement of the X-ray absorption spectrum of a sample from 50 eV below to 1000 eV above the absorption edge (*K*-, *L*- or *M*-edges) of a particular elemental species present in a material, comprises two complementary techniques, *viz*. X-ray absorption near-edge structure (XANES) and extended X-ray absorption fine structure (EXAFS). The former sheds light on the oxidation state of that particular element whereas the latter provides relevant information regarding the bond lengths and the coordination numbers of the neighbouring shells around the elemental species in the material as well as regarding the disorder (both thermal and structural) present in the system. This technique has the added advantage of being element-specific and crystallinity of sample is not a prerequisite. With X-rays being fairly penetrating in matter, this technique is not inherently surface-sensitive and average bulk information from a sample can be obtained. With the advent of modern bright synchrotron radiation sources, this technique has emerged to be one of the most powerful techniques for local structure determination, which can be applied to any type of material, *viz*. amorphous, polycrystalline,

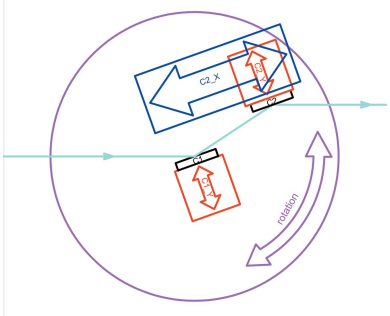

polymers, surfaces and solutions under different ambient and extreme environmental conditions (Koningsberger, 1988; Bunker, 2010; Kelly *et al.*, 2008). XAS beamlines are some of the most significant and extensively used experimental facilities at synchrotron radiation sources all over the world.

Generally, XAS beamlines employ energy selection by step-by-step scanning of a double-crystal monochromator (DCM) along with collection of flux by an ionization chamber or a solid-state fluorescence detector to generate the X-ray absorption spectrum, and hence the time required to record a typical XAS spectrum varies between 10 and 15 min for concentrated samples or standard foils in transmission mode to 1–2 h for dilute samples in fluorescence mode. The recording time also depends on the hardware, required resolution, acceptable noise level and number of data points in a scan. However, an important aspect of the synchrotron-based XAS technique is its capability to perform time-resolved studies under various environments since hard X-rays can pass through highly absorbing sample environments (liquid cells, high-pressure and/or high-temperature cells, chemical reactors, *etc.*). Time-resolved XAS is particularly suitable for monitoring initial nucleation and growth of nanostructures (Ohyama *et al.*, 2010; Polte *et al.*, 2010), since other techniques like transmission electron microscopy (TEM) need a special sample environment and thus cannot be employed for *in situ* characterization. Techniques like UV–Vis spectroscopy and small-angle X-ray scattering can also be employed for *in situ* measurements; however, all these techniques mostly yield information on real-time changes in particle sizes only and cannot throw light on the evolution of the reduction process that is mainly responsible for the nucleation and growth of nanoparticles in such a system. *In situ* XAS measurements, apart from giving quantitative information on the reduction process, can also yield information on the coordination of atoms in clusters which are formed in the initial phase of the growth and act as seeds for further growth of the nanoparticles which cannot be obtained from other techniques. Time-resolved XAS studies are also important for the structural analysis of active sites of heterogeneous catalysts under actual reaction conditions because the reaction gases present in the catalytic systems do not interfere with hard X-rays (Iwasawa, 2003). Measurement techniques which are generally employed to reduce the data collection time in XAS and to enable the time-resolved XAS measurement using synchrotron radiation are (i) energy-dispersive mode (Pascarelli *et al.*, 1999; Bhattacharyya *et al.*, 2009; Matsushita *et al.*, 1986) and (ii) quick-XAS mode (Richwin *et al.*, 2001; Frahm *et al.*, 2005; Tanida *et al.*, 2011). In an energy-dispersive set-up, a long bent crystal is used to focus as well as disperse a band of energy on the sample and the transmitted beam is recorded by a position-sensitive detector, *viz.* a CCD or one-dimensional array detector. The whole XAS spectrum is thus recorded in a single shot and the time resolution is limited by the detector readout time as well as the photon flux available. The dispersive set-up has been implemented in the past to study fast kinetics using a linear photodiode array (Dartyge *et al.*, 1986). Dispersive mode has several advantages: (i) a lack of mechanical movement during acquisition which saves time and prevents vibration-induced noise; and (ii) a focused reflected beam which makes this experiment a spatially localized probe (Buzanich *et al.*, 2016) suited for *in situ* observations (Dartyge *et al.*, 1986; Pascarelli *et al.*, 1999). Successful utilization of the dispersive-EXAFS beamline (BL-08) at INDUS-2 SRS at RRCAT (Indore, India) in monitoring *in situ* growth of Au and Pt nanoparticles has recently been demonstrated (Nayak *et al.*, 2016). However, energy-dispersive set-ups encompass some intrinsic limitations (Bhattacharyya *et al.*, 2009), *viz.* (i) the energy band available for EXAFS measurements at energies <7 keV is very low due to the difficulty in achieving very low radii of curvature by bending a thick crystal; (ii) this technique works in transmission mode only due to the inherent optical scheme and hence samples need microscopic homogeneity throughout the cross section of the beam; and (iii) it does not allow XAS to be measured in total electron yield or fluorescence mode which poses a serious limitation on the samples that can be characterized, *viz.* dilute samples and thin film samples deposited on thick substrates.

On the other hand, the quick-XAS mode of measurement uses a conventional set-up with a DCM, which is subjected to a continuous scan over the energy or angle range required, instead of a conventional step-by-step scan during acquisition of the XAS data. This configuration does not have the limitations encountered with the energy-dispersive geometry and resolution is also comparable with step-by-step scanning; however, the time resolution achievable is typically a few seconds per spectrum. The data acquisition time of the quick-XAS technique has subsequently been reduced to lower than 1 s using two different variants of the set-ups. The first one is piezo-based quick-XAS (Richwin *et al.*, 2001), which is able to collect data in a limited energy region in less than 10 ms and is useful only for time-resolved XANES measurement; the second one is cam-driven quick-XAS (Frahm *et al.*, 2005) mode, where a data acquisition time of 12.5 ms per scan can be achieved with no constraint on energy range. In both the above set-ups, to reach this time resolution, a channel-cut monochromator is utilized, moved by a piezoelectric motor (Richwin *et al.*, 2001) or a cam-driven eccentric (Frahm *et al.*, 2005). However, the increase in time resolution for quick-XAS in the above set-ups has been accompanied by disadvantages such as the loss of the fixed exit, which is dictated by the range of the piezoelectric transducer or the available eccentrics, and good photon statistics or noise on these time scales require a very high flux of the order of 10^{14}–10^{15} photons s^{-1} which is only available at third-generation synchrotron sources.

The Energy-Scanning EXAFS beamline (BL-09) at the INDUS-2 synchrotron source is built on a bending-magnet port with the calculated flux at the sample position being $\sim 10^{11}$ photons s^{-1} at 10 keV (Basu *et al.*, 2014; Poswal *et al.*, 2014) and hence an alternative technique based on a continuous scan of the DCM and on-the-fly measurement of incident and transmitted intensities has been adopted here to carry out quasi-quick-XAS measurements which are presented in this manuscript. The motivation for adopting this scheme came from the realisation that a large fraction of the time needed for

a conventional step-by-step XAS scan is spent waiting for the monochromator mechanics to move from one position to another, for mechanical vibrations due to motions of the main goniometer and second crystal to settle down and for the readout of motor encoders. The settling time depends on the difference between initial and destination positions in the steps as well as on the speed of the movement. The higher the speed, the longer the time required for the vibration to settle down. So, an average of 0.5–2 s are spent in reaching the next step and settling down depending on whether the energy steps are near the absorption edge where the measurements are generally performed in smaller steps or far beyond the edge where the measurements are made in larger steps. Once the movement and vibrations of the crystals are completely stopped, the data are collected which typically takes less than 1 s. Thus the time taken for detection of photons is generally a small fraction of the total time of scanning in an XAS measurement.

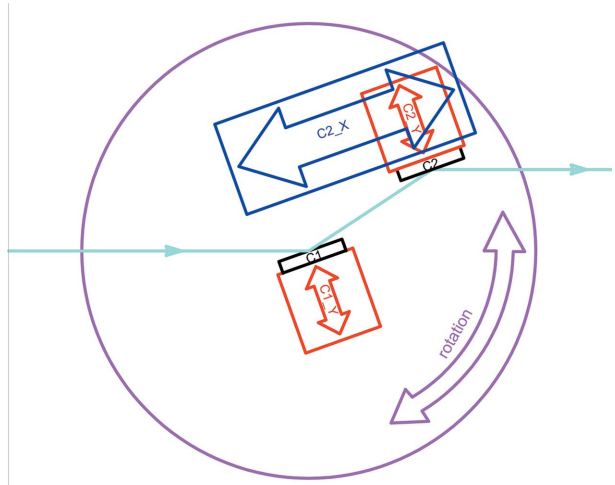

Figure 1
Schematic of the fixed-exit double-crystal monochromator (DCM) with various translation motions and rotation motion.

2. Hardware and data acquisition

As has been mentioned above, the Energy-Scanning EXAFS beamline (BL-09) at INDUS-2 is equipped with a fixed-exit DCM having two silicon (111) crystals. The first crystal is flat and the second crystal has a bending option in the sagittal plane for focusing in the horizontal direction. For focusing in the vertical direction, a cylindrical grazing-incidence mirror is used after the DCM, while another mirror prior to the DCM is used to obtain a collimated beam at the first crystal. The minimum spot size achievable with vertical focusing using the post-mirror and horizontal focusing using the second crystal of the DCM at the sample position is approximately 500 µm × 500 µm.

In a DCM, energy selection is made by setting both the crystals simultaneously at a particular Bragg angle corresponding to the required energy and maintaining their parallelism, with the first-crystal top surface always coinciding with the centre of the goniometer. To achieve a fixed exit height (h) between the incoming and outgoing beam in a DCM over the whole scanned energy range, the distance between the first and second crystal is adjusted using translation of the second crystal perpendicular to the crystal surfaces. The second-crystal vertical distance (C2_Y) from the goniometer centre as shown in the schematic diagram of the DCM (Fig. 1) is given by the following relation,

$$\text{C2\_Y} = \frac{h}{2\cos\theta}, \tag{1}$$

where θ is the Bragg angle which is calculated as follows for silicon (111) crystal at room temperature,

$$\theta = \sin^{-1}\left(\frac{12398.424}{2 \times 3.1356 \times E}\right), \tag{2}$$

where the energy (E) is in electron volts (eV).

As the goniometer angle is changed to change the energy, the beam reflected from the first crystal also changes the area of illumination on the second crystal. To make the beam always fall at the centre of the second crystal, the second crystal is translated using the linear stage as shown in Fig. 1. The value of this lateral translation (C2_X) is calculated using the following formula,

$$\text{C2\_X} = \frac{h}{2\sin\theta}. \tag{3}$$

For a fixed exit height of 32 mm of the incident beam, the C2_Y value is changed by less than 100 µm while to make the beam always fall at the centre of the second crystal the C2_X value has to change by ∼10 mm for an energy scan of 1000 eV.

It was observed that there are vibrations in the exit beam when the second crystal is translated in the C2_X direction due to a substantially higher stroke of movement compared with C2_Y and weak links present in the second-crystal mounting mechanism. Hence a settling time is required for mechanical vibrations to settle if C2_X is translated and, as has been discussed above, a large fraction of time for a full XAS scan is spent doing this. In the continuous-scan mode adopted here, on the other hand, energy scanning is peformed only by changing the Bragg angle and C2_Y motion while C2_X movement of the second crystal is frozen to reduce the vibration of the second crystal. Prior to each XAS scan, C2_X values are calculated for start and end energies and it is fixed at the middle of these two values. Since the length of the second crystal in the direction of the beam is 100 mm and the beam size in the vertical direction is less than 3 mm, this is sufficient to scan the energy around 4 keV required for good XAS data of two adjacent elements in the periodic table. Fig. 2 shows schematically how the DCM can work without moving the second crystal laterally (in the C2_X direction) over a whole energy band of 4 keV. The energy-scanning range depends on the starting energy selected, the vertical acceptance of the DCM and the exit beam height of the incident beam.

Fast and reliable acquisition electronics are also essential to reduce autocorrelation between the spectrum acquisition time and energy resolution. Generally, in the normal step-by-step

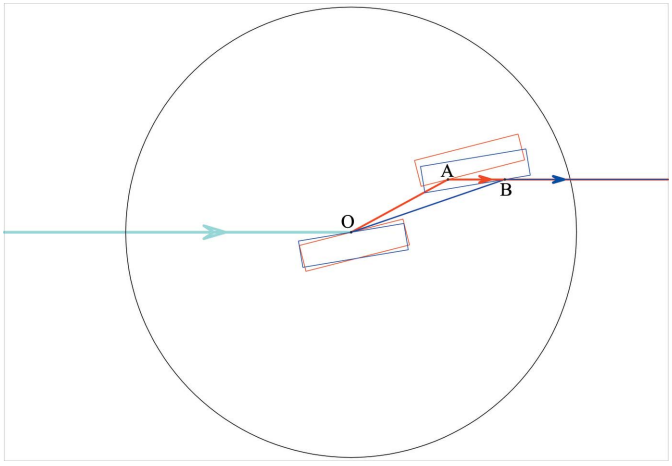

Figure 2
Configuration of the DCM crystals for two energies (8 keV and 12 keV) without moving the second crystal laterally (in the C2_X direction) and constant beam exit height from the incident beam, using 290 µm movement of C2_Y in the vertical direction.

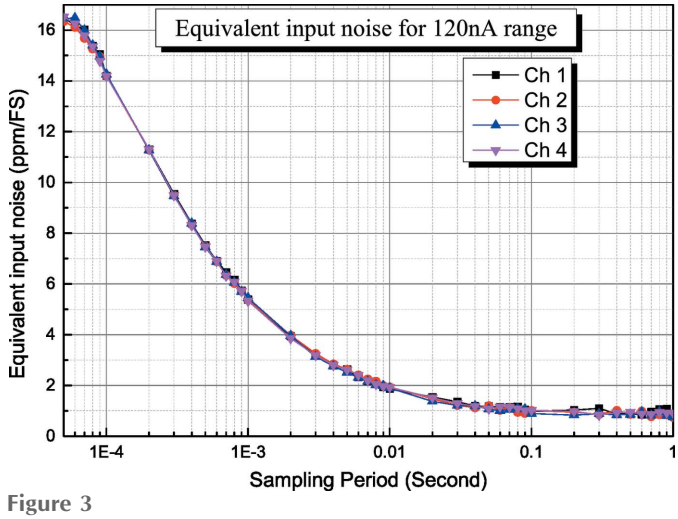

Figure 3
Equivalent input noise of the electrometer measured for 120 nA full range.

energy-scanning mode of the XAS beamlines, the output signals of the ionization chambers are amplified and converted from voltage to frequency (VTF) and these frequencies are recorded using counter timers. This acquisition method shows very good linearity between the signal obtained by the detector and the integration time, but to obtain reliable results it needs a minimum integration time dependent on the range of frequency used by the VTF module. VTF converters up to 100 MHz are commercially available for high-speed data collection in a very short time (Hino *et al.*, 2013), and for the time scale reported for a continuous-mode XAS scan in this manuscript a VTF of 100 MHz would have been suitable. However, with the INDUS-2 synchrotron achieving its full design value of 200 mA in the near future and with more flux available in the beamline, we finally intend to reduce the acquisition time of a full XAS spectrum to 5 s in the continuous-scan mode. Considering the large number of data points to be measured in a full XAS spectrum, the measurement time of a single data point would be less than 100 µs and a VFT converter would possibly not be suitable in that case (Prestipino *et al.*, 2011). Hence we have adopted an alternative mode of measurement in which, for fast data acquisition, ionization current is amplified and directly converted to current values using an analogue-to-digital converter (ADC). In our continuous-scan mode of measurement the current values from the ionization chambers are recorded using a four-channel fast electrometer against the angular positions of the crystals obtained from the angular encoder values of the DCM controller. The four-channel electrometer used here (model TetrAMM from M/s, CAEN ELS, Slovenija) has four independent 24-bit resolution ADCs with an integrated high voltage bias source ranging from 0 V to 4 kV. The sampling frequency of the ADCs remains constant at 100 kHz, but, in order to reduce the noise in the measurement, the samples are averaged. Typical r.m.s. noise for various integration times are shown in Fig. 3. This device can perform bipolar current measurements. The four-channel electrometer input stage is based on four inverting trans-impedance amplifiers (I/V converter) cascaded with particular signal-conditioning stages. The RC time constant is of the order of a few hundred microseconds for fast response to the ionization chamber current measurement. The maximum effective rate by which current from three ionization chambers can be read by the above electrometer is 20 kHz. The current values, measured using the four-channel fast electrometer, are internally synchronized, so there is no synchronization-induced error in measurement while calculating the absorption co-efficient by taking the ratio of incident and transmitted intensities.

In fact, in the above continuous-scan mode, the monochromator rotation speed ($d\theta/dt$) is limited by the minimum acquisition time (Δt), which is associated with the energy sampling (ΔE). This quantity (ΔE) needs to be maintained comparable with or smaller than the intrinsic resolution of the absorption process ($\Delta E_{\rm core}$), as is usually needed for XANES measurements.

At some specific energy E and energy sampling ΔE, the smaller the value of Δt the faster a spectrum can be collected, as shown in the following equation (Prestipino *et al.*, 2011),

$$\begin{aligned}\Delta E = \frac{{\rm d}E}{{\rm d}t}\,\Delta t &= \left[-\left(\frac{hc}{2d}\right)\cot(\theta)\,{\rm cosec}(\theta)\right]\frac{{\rm d}\theta}{{\rm d}t}\,\Delta t \\ &= [-E\cot(\theta)]\frac{{\rm d}\theta}{{\rm d}t}\Delta t \\ &\leq \Delta E_{\rm core}\,, \end{aligned} \quad (4)$$

where d is the inter-planar distance of the monochromator crystal, dE/dt is the speed of the energy scan and θ is the monochromator angle. As has been mentioned above, the maximum continuous acquisition rate (current sampling frequency) for the electrometer can be set at 20 kHz. This shows that the minimum current sampling time (Δt) is 50×10^{-6} s, which enables us to record a spectrum with a minimum energy sampling (ΔE) of less than 0.01 eV with the fastest available monochromator rotation speed of $0.2^\circ\ {\rm s}^{-1}$.

With this speed, a full XAS spectrum can be recorded in less than 10 s.

A computer code based on the PYTHON programming language (https://www.python.org/) has been indigenously developed for acquisition of the continuous-scan data following the above scheme, in the spirit of being simple to use and lower resources on a PC. The *PyEpics* package (http://cars9.uchicago.edu/software/python/pyepics3/) is used in Python to access EPICS (Experimental Physics and Industrial Control System) controls of the various motors and encoders of the DCM. The change of scan speed, the scan range and sampling frequency can be defined by the code. In synchronization to DCM energies, currents from the four-channel electrometer are directly collected on a PC using TCP/IP (Transmission Control Protocol/Internet Protocol). As stated above, during scanning the software uses minimum PC computing power so that synchronization can be maintained between the ionization chamber (IC) currents and energy read by the DCM. During scanning, the software acquires the DCM angle values only and current readings in binary form from the TetrAMM four-channel electrometer. After complete acquisition of data, binary values are converted to ASCII values and are stored in a text file. These output files are multicolumn ASCII files directly usable in the majority of EXAFS analysis software, with a header containing information about the acquisition time, scan parameters and all the positions of the DCM axes during the experiment. This information, written as a header in the ASCII file, can also be used at a later time to check DCM calibration and other trouble-shootings. Subsequent to the collection of the whole data of a scan, current values from ICs and the absorption coefficient with respect to energy is plotted using Python library *Matplotlib* (Hunter, 2007) for visual inspection of the data.

3. Performance test

To illustrate the performance of the beamline in continuous-scan mode and the range covered in a single scan, we have recorded data for three types of systems: (i) standard metal foils of copper and nickel; (ii) a copper–nickel alloy sample; and (iii) a relatively dilute system of silver (Ag) nanocrystals grown in solution phase. There are three main characteristics to demonstrate the performance and precision of this implementation for XAS data collection, namely (i) noise level, (ii) energy resolution and (iii) energy calibration. The average signal-to-noise ratio has been evaluated by the noise-finding function implemented in the *Data Analysis WorkbeNch* (*DAWN*) (Basham *et al.*, 2015). The energy resolution in continuous-scan mode is similar to step-by-step mode since there is no change in the optics and this is shown by recording XAS of standard metal foils. However, the most important part in XAS data collection is energy calibration not only at the edge portion of the spectrum (XANES) but also in the extended region (EXAFS). An imperfect energy calibration or non-linearity of a few eV over 1000 eV above the absorption edge introduces a deviation in the distances of the scatterers from the absorbing atoms from their standard values (Aksenov *et al.*, 2001; Dalba *et al.*, 1999; Pettifer *et al.*, 2005).

3.1. Standard metal foils

One of the main sources of noise in XAS spectroscopy originates from sample inhomogeneity. For this reason, homogeneous metallic foils are used for calibration of energy and testing of performances of XAS beamlines worldwide since these foils are considered as the best approximation to the perfect homogeneous samples. Thus XAS spectra of various standard metal foils were recorded to evaluate the performance of the continuous-scan mode adopted here.

Fig. 4 shows the full XAS spectrum of a Cu foil taken in ~30 s using the continuous mode of measurement discussed above. It should be noted here that, in each scan, data are recorded in forward (μ_f) and reverse direction (μ_r), *i.e.* first with increasing energy and then with decreasing energy. As can be seen from the inset of Fig. 4, there is a slight difference in edge positions between the two spectra which is due to the effect of 'simple moving average' in continuous-scan mode. In the present continuous-scan mode, the energy value is recorded prior to the ionization chamber currents, ionization chambers are normal ionization chambers without grids, and the applied voltage across the electrodes is 400 V. So, these ionization chambers have a delayed response of a few milliseconds (Müller *et al.*, 2013). Owing to the above two reasons, when data are recorded in scans with increasing energy and decreasing energy, there is a shift in absorption spectra of around 0.2 eV. Since this shift has very good repeatability, it can be removed in software itself or taken care of in analysis software. It should be noted here that, although a full XAS spectrum in the present continuous-scan mode can be recorded in less than 10 s using the maximum rotational speed of the DCM goniometer, it has been observed that 30 s is the practical time duration required for a full XAS scan to obtain reasonably good data (with a singal-to-noise ratio of 10^4) over

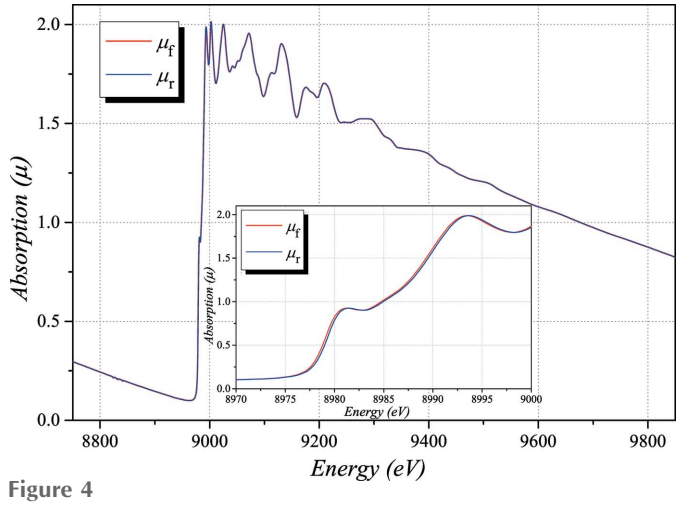

Figure 4
Absorption coefficient (μ) *versus* photon energy (eV) of a standard Cu foil measured in continuous-scan mode. The difference in recorded spectra in increasing energy and decreasing energy scans are shown in the inset.

the complete EXAFS range with the available flux in the beamline. It should be noted that the XANES portions of the spectra can be recorded in less than 5 s. The final energy resolution that can be obtained in an XAS experiment is defined by the width of the thinnest measurable feature in the XANES spectrum (like width of the absorption edge) of a standard metal foil at a chosen energy. In a simplified scheme for an energy-resolution calculation, there are two main components which contribute to broadening of the edge step, namely the intrinsic absorption edge width due to the natural width of the core level, Γ (Krause & Oliver, 1979), and the instrumental resolution due to beamline optics. In this scheme for an energy resolution calculation, each contribution can be considered as having a Gaussian distribution. The resulting overall resolution is simply given by

$$\Delta E = \left[\Gamma^2 + (\Delta E_i)^2\right]^{1/2}. \quad (5)$$

Here, ΔE_i is the instrumental resolution, which depends on the intrinsic resolution of the monochromator reflection and the divergence of the beam. The value of ΔE determined from the FWHM of the first derivative of the Cu *K*-edge absorption spectrum as shown in Fig. 5 is 2.30 eV. By using the natural width of the core level of the Cu *K*-edge as 1.55 eV (Krause & Oliver, 1979), we obtain an instrumental resolution of 1.7 eV at the Cu *K*-edge energy of 8979 eV, which shows very good resolution in the above continuous-scan mode of measurement.

3.1.1. EXAFS data analysis and fitting. Fig. 6 shows the $k^3\chi(k)$ *versus* k spectra of the standard Cu foil derived from the XAS data shown in Fig. 4, from where it can be seen that, for individual scans taken in the continuous mode in ∼30 s, the k-space data up to ∼13 Å^{-1} are sufficiently good and there is hardly any improvement by averaging successive scans. However, there is some improvement in merging the data of several scans beyond 13 Å^{-1} and it can be seen from Fig. 6 that merged data of up to five successive scans is quite comparable up to a k range of 15 Å^{-1} with a scan taken in the step-by-step mode in 15 min. The only difference in the step-by-step and continuous scan is in the amplitude of the oscillations. The step-by-step scan has a slightly larger amplitude compared with the continuous-mode scan.

The above exercise has been carried out for standard Ni foil also. The $k^3\chi(k)$ *versus* k data are subsequently Fourier transformed to obtain the $\chi(R)$ *versus* R data which are finally fitted with theoretically generated spectra using the crystal structure of the respective metals (https://www.fiz-karlsruhe.de/icsd.html). The bond distances (R), co-ordination numbers (N) and disorder (Debye–Waller) factors (σ^2), which gives the mean-square fluctuations in the distances, for the individual paths have been varied while fitting. The best-fit results for the parameters of the first shells of standard Cu and Ni foils for single-scan data taken in continuous mode are shown in Table 1 along with their standard values obtained from X-ray diffraction. It should be noted here that a set of EXAFS data analysis programs available within the *IFEFFIT* software package (Ravel & Newville, 2005) have been used for reduction and fitting of the experimental EXAFS data.

It can be seen from Table 1 that the bond length values obtained from the continuous-scan measurements agree very well with the standard values (Wyckoff, 1963). Generally, the source of error or deviation from the standard values in the EXAFS analysis is due to poor calibration of energy or systematic non-linearity in energy values. If energy is calibrated precisely, the errors in EXAFS can be reduced up to

Table 1
Fitting results for copper and nickel foils with standard R values.

f.c.c. = face-centred cubic.

Foil	σ^2 (Å^2)	R (standard) (Å)	R (fit) (Å)	ΔR (Å)
Copper (f.c.c.) (*Fm3m*)	0.008	2.556	2.551	−0.005
Nickel (f.c.c.) (*Fm3m*)	0.006	2.492	2.495	0.003

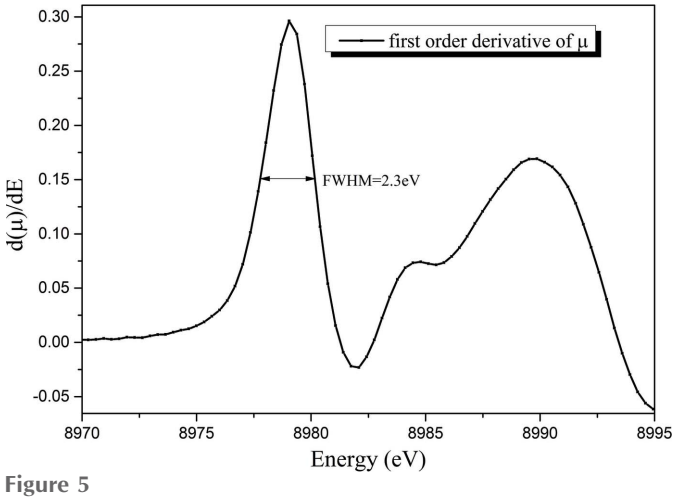

Figure 5
First-order derivative of the absorption spectrum of Cu foil (obtained from Fig. 4).

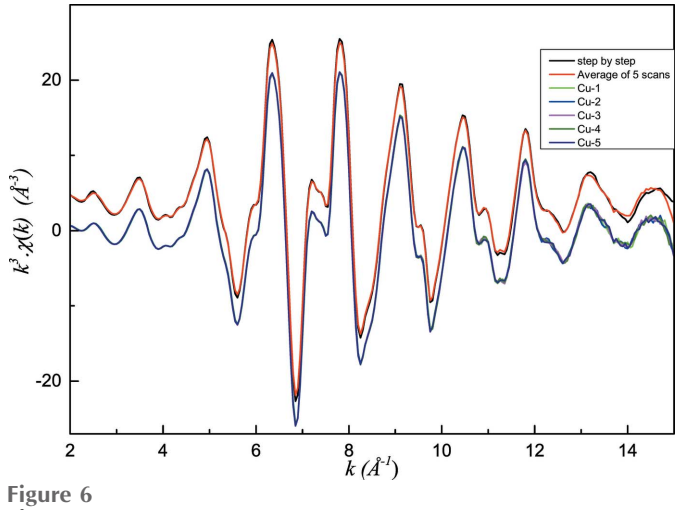

Figure 6
$k^3\chi(k)$ *versus* k plots of the standard copper foil recorded in continuous-scan mode for five successive scans along with an averaged spectrum and a spectrum taken in step-by-step mode. The latter two spectra are shifted up for clear visualization.

10^{-3} Å (Krappe & Rossner, 1999; Pettifer *et al.*, 2005). Our fitting shows a quite satisfactory agreement with standard values which manifests in very good energy calibration for our DCM in continuous-scan mode.

3.2. Copper–nickel–tin alloy

To show the scan range in continuous-scan mode, we chose a copper–nickel–tin (CuNiSn) alloy to measure XAS patterns simultaneously at the Ni and the Cu *K*-edges which are at 8333 eV and 8979 eV, respectively. To cover the XAS spectra of the nickel and copper *K*-edges in a single scan, we recorded the absorption spectra of the alloy from 8200 eV to 10200 eV along with that of a standard copper and nickel foil and the absorption spectra are shown in Fig. 7. In the case of the present CuNiSn alloy, the atomic percentage composition obtained from X-ray fluorescence measurement is as follows: Cu 87.6%, Ni 9.2%, Sn 3.2%. Since the absorption-edge jump also depends on the atomic concentration, the copper and nickel compositional ratio in the sample was also estimated from the relative edge jumps which are found to be 87:9.

3.3. Silver nanoparticles

To demonstrate the capability of the continuous-scan mode of measurement, time-resolved XAS measurement has been carried out to probe the growth of Ag nanoparticles from a solution phase containing $AgNO_3$ precursor. The precursor (100 m*M*) is placed in a glass reaction cell with kapton windows on both sides for passage of X-rays and heated up to 60°C; tri-sodium citrate reducer (500 mM) is injected into it through a motor-driven syringe pump under constant stirring. XAS scans were taken at the Ag *K*-edge starting from the instant of mixing of the reducer, initially every minute with a gap of a few seconds, and later with a gap of 5 min. The time-resolved spectra are shown in Fig. 8 for a few selected instances; XANES as well as the extended part clearly show the reduction process of Ag^+ ions to Ag^o, manifesting in the temporal resolution of the measurement offered by the continuous-scan mode being within a relevant time scale of the reaction kinetics. A complete understanding of the Ag cluster formations during the different stages of growth of Ag nanoparticles from the $AgNO_3$ precursor is presently being investigated by analyzing the EXAFS part of the spectra and will be reported separately.

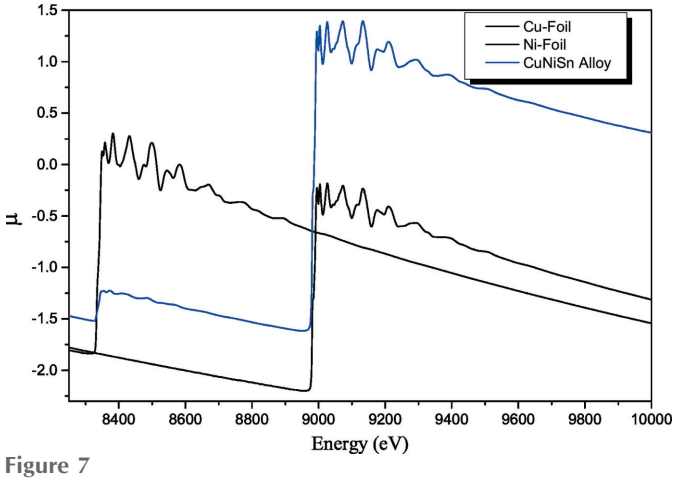

Figure 7
X-ray absorption spectra on Cu and Ni foil and CuNiSn alloy sample at Cu and Ni *K*-edges recorded in a single scan by continuous-scan mode XAS.

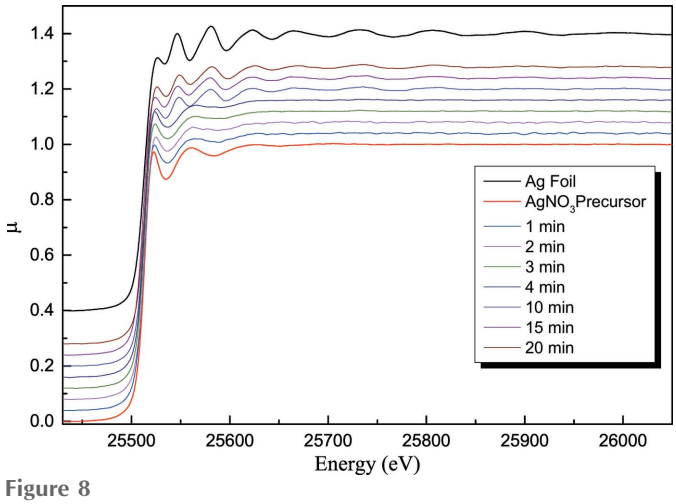

Figure 8
Time-resolved XAS spectra measured at the Ag *K*-edge during reduction of $AgNO_3$ to Ag nanoparticles by tri-sodium citrate. XAS spectra of standard Ag foil and that of the $AgNO_3$ precursor solution are also shown in the figure.

4. Conclusion

A continuous-scan measurement scheme based on restricted movement of the second crystal of the DCM and energy selection by only changing the Bragg angle by simultaneous rotational motion of the two crystals has been implemented in the Energy-Scanning EXAFS beamline (BL-09) of INDUS-2 SRS at RRCAT, Indore, India. Presently, the continuous-scan mode of acquisition offers fast data acquisition of ∼30 s for a full XAS spectrum and less than 5 s for XANES scans and features an excellent signal-to-noise ratio, very good data quality and resolution comparable with step-by-step scanning mode of measurement. This augmentation will help in carrying out time-resolved studies on a variety of systems including *in situ* studies on the growth of nanoparticles and chemical kinetics in heterogeneous catalysis using this beamline. *In situ* time-resolved XAS measurement on the growth of Ag nanoparticles from a solution phase has been carried out in the continuous-scan mode to demonstrate its feasibility in time-resolved probing of structural correlations with reaction kinetics.

References

Aksenov, V. L., Kuzmin, A. Y., Purans, J. & Tyutyunnikov, S. I. (2001). *Phys. Part. Nucl.* **32**, 675–707.
Basham, M., Filik, J., Wharmby, M. T., Chang, P. C. Y., El Kassaby, B., Gerring, M., Aishima, J., Levik, K., Pulford, B. C. A., Sikharulidze, I., Sneddon, D., Webber, M., Dhesi, S. S., Maccherozzi, F., Svensson, O., Brockhauser, S., Náray, G. & Ashton, A. W. (2015). *J. Synchrotron Rad.* **22**, 853–858.

Basu, S., Nayak, C., Yadav, A. K., Agrawal, A., Poswal, A. K., Bhattacharyya, D., Jha, S. N. & Sahoo, N. K. (2014). *J. Phys. Conf. Ser.* **493**, 012032.
Bhattacharyya, D., Poswal, A. K., Jha, S. N., Sangeeta & Sabharwal, S. C. (2009). *Nucl. Instrum. Methods Phys. Res. A*, **609**, 286–293.
Bunker, G. (2010). *Introduction to XAFS: A Practical Guide to X-ray Absorption Fine Structure Spectroscopy*. Cambridge University Press.
Buzanich, A. G., Radtke, M., Reinholz, U., Riesemeier, H. & Emmerling, F. (2016). *J. Synchrotron Rad.* **23**, 769–776.
Dalba, G., Fornasini, P., Grisenti, R. & Purans, J. (1999). *Phys. Rev. Lett.* **82**, 4240–4243.
Dartyge, E., Depautex, C., Dubuisson, J. M., Fontaine, A., Jucha, A., Leboucher, P. & Tourillon, G. (1986). *Nucl. Instrum. Methods Phys. Res. A*, **246**, 452–460.
Frahm, R., Richwin, M. & LtzenkirchenHecht, D. (2005). *Phys. Scr.* **2005**, 974.
Hino, R., Clement, J. M. & Fajardo, P. (2013). *J. Phys. Conf. Ser.* **425**, 212010.
Hunter, J. D. (2007). *Comput. Sci. Eng.* **9**, 90–95.
Iwasawa, Y. (2003). *J. Catal.* **216**, 165–177.
Kelly, S. D., Hesterberg, D. & Ravel, B. (2008). *Methods of Soil Analysis*, Part 5, *Mineralogical Methods*. Madison: Soil Science Society of America.
Koningsberger, D. C. (1988). *X-ray Absorption: Principles, Applications, Techniques of EXAFS, SEXAFS and XANES*. New York: Wiley.
Krappe, H. J. & Rossner, H. (1999). *J. Synchrotron Rad.* **6**, 302–303.
Krause, M. O. & Oliver, J. H. (1979). *J. Phys. Chem. Ref. Data*, **8**, 329–338.
Matsushita, T., Oyanagi, H., Saigo, S., Kaminaga, U., Hashimoto, H., Kihara, H., Yoshida, N. & Fujimoto, M. (1986). *Jpn. J. Appl. Phys.* **25**, L523–L525.
Müller, O., Stötzel, J., Lützenkirchen-Hecht, D. & Frahm, R. (2013). *J. Phys. Conf. Ser.* **425**, 092010.
Nayak, C., Bhattacharyya, D., Jha, S. N. & Sahoo, N. K. (2016). *J. Synchrotron Rad.* **23**, 293–303.
Ohyama, J., Teramura, K., Okuoka, S. I., Yamazoe, S., Kato, K., Shishido, T. & Tanaka, T. (2010). *Langmuir*, **26**, 13907–13912.
Pascarelli, S., Neisius, T., De Panfilis, S., Bonfim, M., Pizzini, S., Mackay, K., David, S., Fontaine, A., San Miguel, A., Itié, J. P., Gauthier, M. & Polian, A. (1999). *J. Synchrotron Rad.* **6**, 146–148.
Pettifer, R. F., Mathon, O., Pascarelli, S., Cooke, M. D. & Gibbs, M. R. J. (2005). *Nature (London)*, **435**, 78–81.
Polte, J., Ahner, T. T., Delissen, F., Sokolov, S., Emmerling, F., Thünemann, A. F. & Kraehnert, R. (2010). *J. Am. Chem. Soc.* **132**, 1296–1301.
Poswal, A. K., Agrawal, A., Yadav, A. K., Nayak, C., Basu, S., Kane, S. R., Garg, C. K., Bhattachryya, D., Jha, S. N. & Sahoo, N. K. (2014). *AIP Conf. Proc.* **1591**, 649–651.
Prestipino, C., Mathon, O., Hino, R., Beteva, A. & Pascarelli, S. (2011). *J. Synchrotron Rad.* **18**, 176–182.
Ravel, B. & Newville, M. (2005). *J. Synchrotron Rad.* **12**, 537–541.
Richwin, M., Zaeper, R., Lützenkirchen-Hecht, D. & Frahm, R. (2001). *J. Synchrotron Rad.* **8**, 354–356.
Tanida, H., Yamashige, H., Orikasa, Y., Oishi, M., Takanashi, Y., Fujimoto, T., Sato, K., Takamatsu, D., Murayama, H., Arai, H., Matsubara, E., Uchimoto, Y. & Ogumi, Z. (2011). *J. Synchrotron Rad.* **18**, 919–922.
Wyckoff, R. W. G. (1963). *The Structure of Crystals*, 2nd ed. New York: Interscience.